

Determination of shear stiffness based on thermal noise analysis in atomic force microscopy: Passive overtone microscopy

Tanja Drobek, Robert W. Stark,* and Wolfgang M. Heckl†

Universität München, Institut für Kristallographie und Angewandte Mineralogie, Theresienstraße 41, 80333 München, Germany

(Received 30 November 2000; published 21 June 2001)

In torsional overtone microscopy, a dynamic atomic force microscopy technique, antisymmetric vibration modes of a v-shaped cantilever are used to investigate the elastic properties of the tip-sample contact. In order to minimize the vibration amplitude, no external excitation is added in the passive overtone mode. In this mode, the thermomechanical noise of the surface coupled cantilever at room temperature is analyzed. This allows the shear stiffness of the tip-sample contact to be extracted from the analysis of the power spectrum of the photodiode signal. The load dependence of the first torsional vibration on silicon, aluminum, and cadmium telluride surfaces is compared with a theoretical mechanical model.

DOI: 10.1103/PhysRevB.64.045401

PACS number(s): 68.37.Ps, 62.20.-x, 62.25.+g, 81.70.-q

I. INTRODUCTION

The combination of high spatial resolution with high force sensitivity in atomic force microscopy (AFM)¹ makes it a suitable instrument for the investigation of elastic properties. The elastic modulus of soft materials can be determined by quasistatic nanoindentation measurements on the nanometer scale.² For stiff materials the accuracy of this method is limited, since small tip radii imply a high contact pressure even at low forces, and therefore the limit of plastic deformation restricts the applicable forces.³ The rate of data acquisition for quasistatic indentation methods is limited by the fundamental resonant frequency of the cantilever, though it is possible to accelerate the quasistatic methods by miniaturizing the probes.⁴ Dynamic methods like fourier transformed force microscopy,^{5,6} ultrasonic force microscopy,⁷⁻¹⁰ and acoustic friction force microscopy^{11,12} take advantage of the effects of tip-sample interactions on the cantilever vibration in order to characterize the sample. In torsional overtone microscopy, an antisymmetric vibration mode of the cantilever is used to achieve image contrast based on the shear stiffness of the tip-sample contact.¹³

In thermodynamic equilibrium the mean-square displacement of the tip from its neutral position is described by

$$\sqrt{\langle u^2 \rangle} = \sqrt{\frac{k_B T}{c_{\text{cant}}}}. \quad (1)$$

Here, u is the z -displacement of the tip, k_B is the Boltzmann constant, T the temperature of the surrounding heat bath, c_{cant} the cantilever spring constant, and $\langle \rangle$ denotes the average in time (cf. e.g.^{14,15}). Therefore the average potential energy of the Brownian motion of the cantilever is $1/2 k_B T$ for each degree of freedom. By measuring the spectral power density and the resonant frequencies of this thermomechanical noise it is possible to calibrate the force constant of the AFM probe.^{14,16,17} Another application of the thermal noise is the investigation of oscillatory hydration potentials and the measurement of viscoelastic parameters of polymers.^{18,19}

Here we report on the investigation of mechanical sample properties by analysis of the thermomechanical noise of the

first antisymmetric eigenmode of the cantilever. In this small amplitude limit of force microscopy, friction effects^{20,21} and nonlinearities²² are minimized. The cantilever used in this experiment has a spring constant of $c_{\text{norm}} = 0.13$ N/m, so in z -direction the free cantilever has a mean square displacement $\sqrt{\langle u_z^2 \rangle} = 1.8$ Å, which is reduced when the tip is in contact with the sample. It has a lateral spring constant of $c_{\text{tor}} = 13.4$ N/m and the lateral mean square displacement $\sqrt{\langle u_y^2 \rangle}$ of the tip from the neutral position at room temperature is

$$\sqrt{\langle u_y^2 \rangle} = \frac{0.64 \text{ Å}}{\sqrt{c_{\text{tor}}}} < 20 \text{ pm}, \quad (2)$$

which is smaller than the typical interatomic distance. This lateral oscillation amplitude is the lower experimental limit achievable in room temperature AFM.

II. MODELING

When the movement of the AFM tip is restricted by the interaction forces between the tip and the sample, the boundary conditions of the cantilever motion change, inducing a node in the vibrational motion at the tip and increasing the resonant frequencies. Due to their different bending shapes, the symmetric and antisymmetric vibration modes are influenced differently by the contact stiffness normal to the sample surface and the lateral stiffness parallel to the sample surface.

In Fig. 1, the principle of the torsional overtone microscopy is shown. The v-shaped cantilever is driven at the resonant frequency of the first antisymmetric (torsional) vibration, where both arms oscillate in opposing directions, giving rise to a torque at the front end of the cantilever. In the case of a free cantilever, the tip executes a lateral motion. In contact with the sample surface, the torque leads to a different bending shape as well as an increase of the resonant frequency of the torsional vibration mode.¹³

Though the contact stiffness in the normal as well as in the lateral directions are not proportional to the loading force, in the small amplitude limit they can be approximated

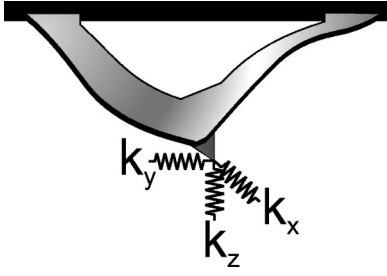


FIG. 1. Principle of passive overtone microscopy. The tip-sample contact is modelled as a tripod of linear springs $k_{\text{lat}/x}$, $k_{\text{lat}/y}$, and k_{norm} attached to the tip. The Brownian motion of the cantilever is detected by an optical-beam setup and investigated with a spectrum analyzer.

as a tripod of linear springs k_{norm} , $k_{\text{lat}/x}$, and $k_{\text{lat}/y}$, which are mounted on the tip apex. The linearized shear stiffness k_{lat} is proportional to the contact radius a ,²³

$$k_{\text{lat}} = 8G^*a, \quad (3)$$

where G^* is the effective shear stiffness of the tip-sample contact, which is calculated from the shear moduli G_i and the Poisson's ratios of the tip and sample materials

$$G^* = \left(\frac{2 - \nu_1}{G_1} + \frac{2 - \nu_2}{G_2} \right)^{-1}. \quad (4)$$

The effective Young's modulus E^* of the tip sampler contact, with respect to Young's moduli E_i , is given by

$$E^* = \left(\frac{1 - \nu_1^2}{E_1} + \frac{1 - \nu_2^2}{E_2} \right)^{-1}. \quad (5)$$

For anisotropic materials, the correction factor $\beta_{(hkl)}$ has to be introduced into the second term²⁴ leading to the indentation modulus

$$M_{(hkl)} = \beta_{(hkl)} \left(\frac{E_{\langle 100 \rangle}}{1 - \nu^2} \right). \quad (6)$$

The Young's modulus $E_{\langle 100 \rangle}$ in $\langle 100 \rangle$ direction of the crystal is easily derived from the components of the elastic tensor²⁵

$$E_{\langle 100 \rangle} = s_{11}^{-1}. \quad (7)$$

The effective shear modulus is calculated from the shear moduli G_i of tip and sample by Eq. (4). The shear modulus is calculated from the components s_{ij} of the elastic tensor²⁵

$$G = [2(s_{11} - s_{12})]^{-1}. \quad (8)$$

Since different material properties, such as elasticity and adhesion, contribute to the interaction between tip and sample, there is no general description of the contact mechanics. The conditions of the contact can be characterized by the parameter μ , which represents the ratio of the elastic displacement of the surfaces at the point of separation (pull-off) to the effective range of the surface forces²⁶

$$\mu = \left(\frac{RW^2}{E^*z_0^3} \right)^{1/3}. \quad (9)$$

Here, z_0 is the equilibrium separation of the Lennard-Jones potential, R is the tip radius, and W the work of adhesion. For stiff materials with small long-range attractive forces, i.e. for $\mu < 0.1$, the contact mechanics is described by Dejarguin, Müller, and Toporov (DMT),^{27,28} whereas for $\mu > 5$, in the case of compliant materials with large, short-range attractive forces, the Johnson-Kendall-Roberts model (JKR) can be applied.²⁹ Though in between both extremes the adequate description is given by the Maugis-Dugdale model (MD),³⁰ it was shown that for $\mu > 0.3$, the radius of contact is well predicted by the JKR model.²⁶ In the experiment reported here, the values of μ are in the range of 0.34 to 0.56, thus the JKR model was used for the interpretation of the experimental data.

In the framework of the JKR²³ theory the contact radius is given by

$$a = \left[\frac{3R}{4E^*} (P + 3\pi RW + \sqrt{6\pi RWP + (3\pi RW)^2}) \right]^{1/3}. \quad (10)$$

Here, P is the normal load pressing the tip into the surface. The work of adhesion W can be determined experimentally by measuring the pull-off force P_{sep} , which is necessary to separate tip and sample,²⁹

$$P_{\text{sep}} = -1.5\pi WR. \quad (11)$$

In order to get a realistic description of the mechanical behavior of the system, the cantilever was modeled by finite element analysis (FEA). The finite element analysis was carried out using the static and modal analysis tools of the commercial software package ANSYS 5.4 running on an IBM-SP2 workstation at the Leibniz Rechenzentrum, München, Germany. The resonant spectrum of the v-shaped cantilever was calculated solving the eigenvalue problem

$$\mathbf{M}\ddot{\mathbf{u}} + \mathbf{C}\dot{\mathbf{u}} + \mathbf{K}\mathbf{u} = \mathbf{0}. \quad (12)$$

\mathbf{M} and \mathbf{K} are the mass and the stiffness matrix, \mathbf{C} is the damping matrix, and \mathbf{u} denotes the nodal translation vector. The influence of the tip-sample contact is introduced into the model as a tripod of linear springs connected to the tip. Since the boundary conditions are not time dependent, they are integrated in the stiffness matrix \mathbf{K} . In order to avoid an unrealistic deformation of the tip in the FEA model, each spring was divided into 65 separate parallel springs, connected to each node of the tip, which was modeled as a cut off pyramid. The cantilever model was built up as a mesh of 4062 nodes, consisting of a single material component. For the correct section moment, the Young's modulus of this material was reduced,³¹ whereas the Poisson's ratio was in-

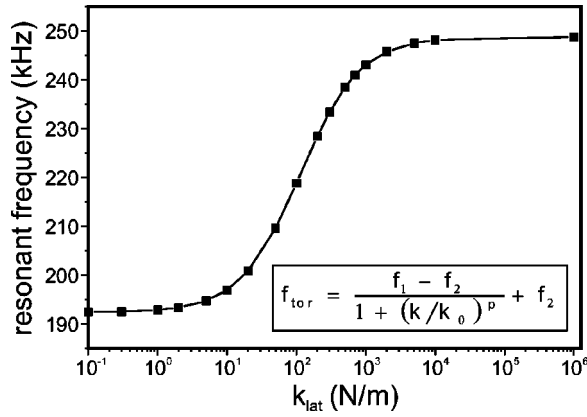


FIG. 2. Calculated resonant frequency (squares) of the first torsional vibration mode versus spring constants of the lateral springs ($k_{lat/x}$, $k_{lat/y}$). An empirical Logistic function (solid line, parameters $k_0=113.0$ N/m, $f_1=192.3$ kHz, $f_2=248.8$ kHz, $p=1.004$) is a good approximation for the FEA data.

creased to reproduce the resonant frequencies of the torsional vibration modes. In this procedure, the different experimentally determined values of the damping were taken into account, which lead to a shift of the resonant frequencies. Mesh refinement was performed in order to verify the mesh independence of the solutions.

The result of the modal analysis is shown in Fig. 2. The resonant frequency f_{tor} of the first antisymmetric mode is plotted against the shear stiffness k_{lat} of the tip-sample contact. Since f_{tor} is independent of k_{norm} , a value of 100 N/m was used for the normal springs, which is a typical value for the contact stiffness of an AFM tip on an aluminum surface. The value for f_{tor} versus the lateral spring constant is fitted empirically by the logistic function

$$f_{tor} = \frac{f_1 - f_2}{1 + \left(\frac{k_{lat}}{k_0}\right)^p} + f_2, \quad (13)$$

with the parameters $k_0=113.0$ N/m, the frequency of the free cantilever torsion $f_1=192.3$ kHz, the frequency of the cantilever torsion with a clamped tip $f_2=248.8$ kHz, as well as an exponent $p=1.004$. This fitting function has a symmetric sigmoidal shape on a logarithmic scale. Using Eq. (13) the lateral stiffness of the tip-sample contact is derived from the shift of the resonant frequency.

III. EXPERIMENTAL

The spectral density of the thermomechanical noise of the AFM photodiode signal was measured with the tip in contact to different sample surfaces. Quasistatic cycles of loading and unloading were carried out in order to investigate the dependence of the lateral stiffness from the contact radius. Between the loading and unloading steps, and data acquisition, a time interval of 90 s was added for relaxation.

The data were obtained with a modified commercial AFM instrument in ambient conditions (Topometrix Explorer, dry scanner, 130 μm scan range and 10 μm z -range). The de-

flexion of the cantilever was detected by an optical lever system and a quadrant photodiode. The frequency spectra of the thermal noise were measured with a spectrum analyzer (HP E 4402 B, ESA-E series). The respective work of adhesion was determined from a series of quasistatic force-distance curves on the samples. All experiments were performed with a single cantilever (Park Scientific Instruments, sharpened Microlever, gold-coated Si_3N_4 , v-shaped, nominal spring constant $c=0.1$ N/m, measured spring constant $c=0.13$ N/m, resonant frequency nominal $f_0=38$ kHz, and measured 31.5 kHz). The exact geometry of the cantilever used in the experiment was obtained from a detailed SEM analysis.³² The thickness of the gold layer was measured with the AFM on an edge produced by partially removing the coating.

In the experiment three different samples were investigated. The surface of a silicon (100) wafer, a piece of polycrystalline aluminum (Topometrix test sample), and the (100) surface of a cubic Cadmium Telluride (CdTe) single crystal. An isotropic approach was used for the calculation of the effective shear stiffness G^* .

IV. RESULTS AND DISCUSSION

The spectral density of the thermomechanical noise of the cantilever in the frequency range from 180 kHz to 230 kHz for several loading forces on the aluminum sample is shown in Fig. 3. Curve (1) is the torsional resonance of the free cantilever with a resonant frequency of $f_1=192.8$ kHz. The contact resonances [curves (2) to (7)] were measured increasing the loading force P stepwise. While the peak intensity decreases at higher loading forces, the torsional resonant frequency is shifted towards higher frequencies. Here the higher loading forces cause an expansion of the contact region and therefore an increase of the lateral stiffness k_{lat} , leading to a frequency shift of the torsional resonance as predicted by modal analysis [cf. Fig. (2)]. For a detailed analysis, the frequency shifts were determined by fitting a resonance peak to the spectral density data. With Eq. (13), the lateral stiffness values were calculated from the measured frequency shifts.

The lateral stiffness measured during approach/retract cycles on the Al, Si, and CdTe samples is presented in Fig. 4, plotted versus the loading force P . The data were fitted using Eq. (10) and Eq. (3), achieving experimental values for the reduced shear stiffness G^* as a fit parameter. The results of the fitting procedure are listed in Table I. With an effective tip radius of 24 nm and the reduced shear stiffness G^* calculated from the literature data,³³ the fitting curve of the JKR model reproduces the experimental data very well. For a quantitative deviation of the shear stiffness, the data achieved on the aluminum surface was taken as a calibration standard for the interpretation of the data measured on the other samples.

For the silicon data, a fit with the same effective tip radius leads to a reduced shear stiffness value, which is about 10% smaller than the calculated value. Due to the higher rigidity of the silicon material, uncertainties in the elastic constants of the tip material as well as deviations from the ideal spherical geometry show a stronger influence on the real area of

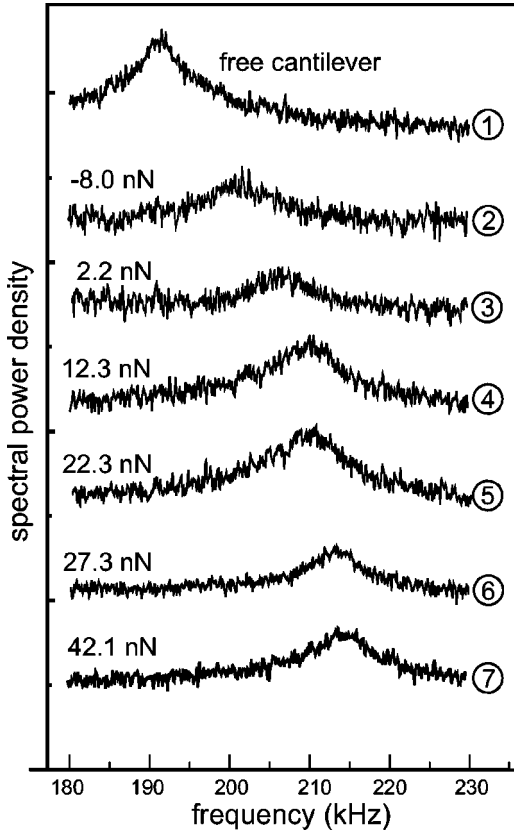


FIG. 3. Noise spectra of the first torsional vibration. (1) free cantilever, (2)-(7) surface coupled cantilever (aluminum sample). The loading force P was increased step-by-step as indicated.

contact than on compliant materials.

For the cadmium telluride sample the experimental value is about 3% higher than the literature data. The CdTe sample also shows nonelastic effects: in Fig. 4, the dotted line is connecting the lateral stiffness data measured in an approach retract cycle. The arrow indicates the beginning of a hysteric behavior, starting at a loading force of $P > 21$ nN explained by the transition from elastic to plastic deformation. From JKR theory, the contact radius is $a = 3.8$ nm. Therefore, the average pressure is about 470 MPa, while the maximum pressure at the tip apex is 690 MPa.²³ This value is comparable to a Mohs' hardness of 600 MPa reported for cubic CdTe.³⁴ The deviations from values obtained by macroscopic methods are presumably caused by a nonideal tip shape. In the approach direction, contact softens at the occurrence of plastic yielding. In retraction, the area of contact between tip and sample is increased, leading to a stiffened effective contact. Thus, for a determination of elastic parameters, only values in approach direction, before the onset of yield, were used.

V. CONCLUSIONS

An alternative approach for the determination of elastic sample properties by atomic-force microscopy has been introduced here. In order to minimize the tip amplitude and thus avoid nonlinearities and friction effects in the tip-

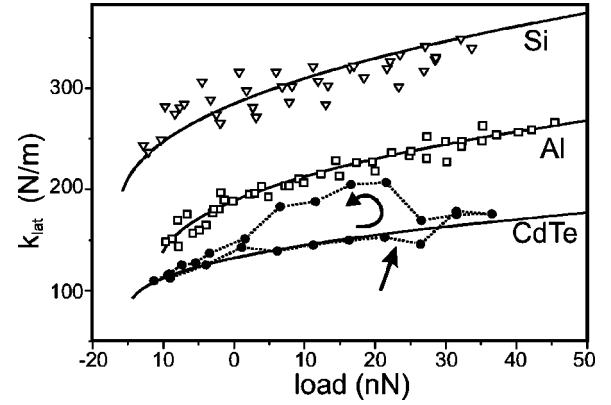


FIG. 4. Lateral stiffness determined from the resonant frequencies of the first torsional vibration as obtained from noise spectra in contact with Si, Al, and CdTe surfaces versus the loading force P . The data were fitted using the JKR model (solid lines) for $G_{\text{Si}}^* = 14.4$ GPa, $G_{\text{Al}}^* = 9.6$ GPa, and $G_{\text{CdTe}}^* = 4.6$ GPa. The dotted line shows an approach retract cycle on CdTe (curved arrow). The onset of the hysteric behavior is indicated with an arrow. Note the apparent softening due to plastic deformation, as well as the higher stiffness in retraction caused by an enlarged contact area.

sample contact, only passive thermal excitation was exploited. Analyzing the spectral density of the thermomechanical fluctuations attributed to the first antisymmetric (torsional) vibrational mode of the surface-coupled cantilever, the shear stiffness of the specimen was obtained. The experiment shows that passive torsional overtone microscopy is a quantitative method for the determination of nanomechanical properties with high spatial resolution. Additionally, it can be applied to quasistatic indentation measurements, where it provides complementary information on the mechanical contact properties. It also should be

TABLE I. Experimental data of the effective shear modulus for silicon, aluminum, and cadmium telluride G^* in comparison with the values calculated from the material parameters reported in literature. The tip was modeled using the elastic constants of amorphous silicon nitride. The pull-off force P_{sep} was determined from force-distance curves.

	Si	Al	CdTe	Si_3N_4 ^a
G_{exp}^* (GPa)	14.4	9.6	4.6	
G_{calc}^* (GPa)	15.9	9.6	4.5	
E^* (GPa)	75.6	50.2	22.1	
$E_{<100>}$ (GPa)	129	63.3	23.4	170
G_{calc} (GPa)	50.5	23.1	8.3	60
ν	0.28	0.36	0.41	0.27
s_{11} (TPa^{-1}) ^b	7.74	15.8	42.7	
s_{12} (TPa^{-1}) ^b	-2.17	-5.8	-17.4	
s_{44} (TPa^{-1}) ^b	12.6	35.8	49.5	
β ^c	0.92	0.95	0.89	
P_{sep} (nN)	16.2	10.7	14.8	

^aReference 31.

^bReference 33.

^cReference 24.

possible to make use of the method for single molecule force spectroscopy experiments in order to obtain further information on viscoelastic properties.³⁵ For an extensive analysis of the contact properties, other resonances can also be analyzed.

ACKNOWLEDGMENTS

We thank Agilent GmbH Germany for supplying the spectrum analyzer for test purposes. This work was supported by DFG Grant He-1617/7-1 (TD) and BMBF (RWS).

*Present address: Nanotechnology Group, Swiss Federal Institute of Technology, ETH-Center/CLA, CH-8092 Zürich, Switzerland.

†Corresponding author: Tel. Fax: ++49-(0)89-2394-4331, Email address: heckl@lrz.uni-muenchen.de

- ¹G. Binnig, C.F. Quate, and C. Gerber, *Phys. Rev. Lett.* **56**, 930 (1986).
- ²B. Capella and G. Dietler, *Surf. Sci. Rep.* **34**, 1 (1999).
- ³R.W. Carpick and M. Salmeron, *Chem. Rev.* **97**, 1163 (1997).
- ⁴M.B. Viani, T.E. Schäffer, and G.T. Paloczi, *Rev. Sci. Instrum.* **70**, 4300 (1999).
- ⁵R.W. Stark and W.M. Heckl, *Surf. Sci.* **457**, 219 (2000).
- ⁶M. Stark, R.W. Stark, W.M. Heckl, and R. Guckenberger, *Appl. Phys. Lett.* **77**, 3293 (2000).
- ⁷K. Yamanaka, H. Ogiso, and O. Kolosov, *Appl. Phys. Lett.* **64**, 178 (1994).
- ⁸K. Yamanaka, A. Noguchi, T. Tsuji, T. Koike, and T. Goto, *Surf. Interface Anal.* **27**, 600 (1999).
- ⁹U. Rabe and W. Arnold, *Appl. Phys. Lett.* **64**, 1493 (1994).
- ¹⁰U. Rabe, S. Amelio, E. Kester, V. Scherer, S. Hirsekorn, and W. Arnold, *Ultrasonics* **38**, 430 (2000).
- ¹¹K.J. Wahl, S.V. Stepnovski, and W.N. Unertl, *Tribol. Lett.* **5**, 103 (1998).
- ¹²V. Scherer, W. Arnold, and B. Bhushan, *Surf. Interface Anal.* **27**, 578 (1999).
- ¹³T. Drobek, R.W. Stark, M. Gräber, and W.M. Heckl, *New J. Phys.* **1**, 15 (1999).
- ¹⁴J.L. Hutter, J. Bechhoefer, *Rev. Sci. Instrum.* **64**, 1868 (1993).
- ¹⁵P. Saulson, *Phys. Rev. D* **42**, 2437 (1990).
- ¹⁶H.J. Butt and M. Jaschke, *Nanotechnology* **6**, 1 (1995).
- ¹⁷R.W. Stark, T. Drobek, and W.M. Heckl, *Ultramicroscopy* **86**, 207 (2001).
- ¹⁸J.P. Cleveland, T.E. Schäffer, and P.K. Hansma, *Phys. Rev. B* **52**, R8692 (1995).
- ¹⁹A. Roters, M. Gelbert, M. Schimmel, J. Rühle, and D. Johannsmann, *Phys. Rev. E* **56**, 3256 (1997).
- ²⁰J.J. Chen, B.D. Yang, and C.H. Menq, *J. Sound Vib.* **229**, 775 (2000).
- ²¹H.K. Hong and C.S. Liu, *J. Sound Vib.* **229**, 1171 (2000).
- ²²M. Troyon, Z. Wang, D. Pastre, H.N. Lei, and A. Hazotte, *Nanotechnology* **8**, 163 (1997).
- ²³K.L. Johnson, *Contact Mechanics* (Cambridge University Press, Cambridge, 1985).
- ²⁴J.J. Vlassak and W.D. Nix, *J. Mech. Phys. Solids* **42**, 1223 (1994).
- ²⁵J.F. Nye, *Physical Properties of Crystals* (Oxford Science Publications, Oxford, 1985).
- ²⁶K.L. Johnson and J.A. Greenwood, *J. Colloid Interface Sci.* **192**, 326 (1997).
- ²⁷B.V. Derjaguin, V.M. Müller, and Y.P. Toporov, *J. Colloid Interface Sci.* **53**, 314 (1975).
- ²⁸V.M. Müller, B.V. Derjaguin, and Y.P. Toporov, *Colloids Surface* **7**, 251 (1983).
- ²⁹K.L. Johnson, K. Kendall, and A.D. Roberts, *Proc. R. Soc. London, Ser. A* **324**, 301 (1971).
- ³⁰D. Maugis, *Rev. Metall./Cah. Inf. Tech.* **94**, 655 (1997).
- ³¹J. Hazel and V. Tsukruk, *Thin Solid Films* **339**, 249 (1999).
- ³²Nanotools GmbH, SEM Certificate, Technical report, LMU Munich, 2000 (unpublished).
- ³³Landolt-Börnstein in *Zahlenwerte und Funktionen aus Naturwissenschaften und Technik*, edited by K.H. Hellwege and A.M. Hellwege, Vol. 11 (Springer-Verlag, Berlin, 1979).
- ³⁴CRS, *Handbook of Chemistry and Physics*, 70th ed. (CRC, Boca Raton, Florida, 1989).
- ³⁵M. Rief, F. Oesterhelt, B. Heymann, and H.E. Gaub, *Science* **275**, 1295 (1997).